EUROPEAN ORGANIZATION FOR NUCLEAR RESEARCH

Conf-820718--17

DOE/ER/40033--32

DE83 002451

CERN-EP/82-133
23 August 1982

Rockefeller University
Report No. DOE/ER/40033-32

(RU 81/A-30)

DETERMINATION OF THE ANGULAR AND ENERGY DEPENDENCE OF HARD CONSTITUENT SCATTERING FROM π^0 PAIR EVENTS AT THE CERN INTERSECTING STORAGE RINGS

CERN[1]-Columbia[2]-Oxford[3]-Rockefeller[4] (CCOR) Collaboration

A.L.S. Angelis[3)], H.-J. Besch[1)], B.J. Blumenfeld[1,2,*)], L. Camilleri[1)], T.J. Chapin[4)], R.L. Cool[4)], C. del Papa[1,**)], L. Di Lella[1)], Z. Dimčovski[4,***)], R.J. Hollebeek[2,†)], L.M. Lederman[2,††)], D.A. Levinthal[2)], J.T. Linnemann[4)], C.B. Newman[1,†††)], N. Phinney[1,3,†)], B.G. Pope[1,†††)], S.H. Pordes[1,4,††)], A.F. Rothenberg[4,1)], R.W. Rusack[2,×××)], A.M. Segar[3)], J. Singh-Sidhu[1,+)], A.M. Smith[1)], M.J. Tannenbaum[4,++)], R.A. Vidal[2,†)], J.S. Wallace-Hadrill[3)], J.M. Yelton[3,†)] and K.K. Young[1,+++)]

1) CERN, Geneva, Switzerland
2) Columbia University[×)], New York, NY, USA
3) University of Oxford, Oxford, UK
4) The Rockefeller University[××)], New York, NY, USA

Submitted to the
21st International Conference on High-Energy Physics
Paris, 26-31 July 1982

---

*) Present address: Physics Dept., Johns Hopkins University, Baltimore, Md., USA.
**) Present address: INFN, Sezione di Bologna, Italy.
***) Present address: University of Skopje, Macedonia, Yugoslavia.
†) Present address: SLAC, Stanford, Calif., USA.
††) Present address: Fermilab, Batavia, Ill., USA.
†††) Present address: Physics Dept., Princeton University, Princeton, NJ, USA.
+) Present address: Physics Dept., University of Manchester, UK.
++) Present address: Brookhaven National Laboratory, Upton, NY, USA.
+++) Permanent address: Physics Dept., University of Washington, Seattle, Wash., USA.
×) Research supported in part by the National Science Foundation.
××) Research supported in part by the US Department of Energy.
×××) Present address: Rockefeller University, New York, NY, USA.

DISCLAIMER

THIS PAGE

WAS INTENTIONALLY

LEFT BLANK

ABSTRACT

We present data on proton-proton collisions, obtained at the CERN Intersecting Storage Rings, in which two roughly back-to-back π^0's of high transverse momentum (p_T) were produced. The angular distribution of the dipion axis relative to the collision axis is found to be independent of both the effective mass m of the dipion system and the centre-of-mass energy $\sqrt{s}$ of the proton-proton collision. The cross-sections $d\sigma/dm$ at the two values of $\sqrt{s}$ satisfy a scaling law of the form $d\sigma/dm = G(x)/m^n$, where $x = m(\pi^0,\pi^0)/\sqrt{s}$ and $n = 6.5 \pm 0.5$. We show from our data that the leading π^0 carries most of the momentum of the scattered parton. Given this fact, the axis of the dipion system follows closely the direction of the scattered constituents, and we exploit this to determine the angular dependence of the hard-scattering subprocess. We also compare our data with the lowest order QCD predictions using structure functions as determined in deep-inelastic scattering and fragmentation functions from electron-positron annihilation.

The CCOR Collaboration has been performing a general study of high transverse momentum phenomena in pp collisions at the CERN Intersecting Storage Rings (ISR) [1-7]. In this paper we present data on events in which two roughly back-to-back π^0's, each of high transverse momentum [$2.5 < p_T(\pi^0) < 8$ GeV/c], were detected. It has been argued [8] that the cross-section for this type of symmetric process is 'determined directly' by the hard-scattering subprocesses and, compared to the single-particle high-p_T cross-section, is relatively insensitive to the so-called primordial or intrinsic transverse momentum of the incident partons. The π^0's were detected in two arrays of lead-glass Čerenkov counters centred at 90° on either side of the interaction region. Each array covers a polar angle θ of ±30° around 90°, and an azimuthal angle ϕ of ±20° around the median plane. They sit outside an axial superconducting solenoid magnet which contains a set of drift chambers used to determine the momenta of charged particles over the full azimuth in a polar angle range of ±37° around 90°.

The experiment used two independent triggers. One, the "pairs" trigger, required that at least 2.5 GeV of energy be deposited in any 3 × 3 matrix of counters in each lead-glass array; the other, the "inclusive" trigger required a similarly localized energy deposition above 7 GeV in either array. Details of the apparatus and method have been given previously [1-7]. The data come from an integrated luminosity of 1.7×10^{37} cm^{-2} at $\sqrt{s}$ = 44.8 GeV, and of 9.2×10^{37} cm^{-2} at $\sqrt{s}$ = 62.4 GeV.

The data are presented using the following kinematic variables: m, the invariant mass of the $\pi^0\pi^0$ system; $\cos\theta^*$, the average of the cosines of the polar angles between the π^0's and the proton-proton axis in the frame where the dipion system has no net longitudinal momentum*); Y, the rapidity of the dipion system

---

*) The reference frame used is found by transforming only along the original collision axis. If the π^0's have different transverse momenta, the two polar angles, θ^{**}, are unequal; $\cos\theta^*$ is defined as the average of the cosines. For small net P_T, as required in this analysis, all definitions (Collins-Soper, Gottfried-Jackson, etc.) become approximately the same. We have deliberately not transformed away the net P_T of the dipion system, since this is affected by the jet fragmentation process. Our averaging procedure should be less sensitive to biases from this effect.

in the pp centre of mass; and P_T, the net transverse momentum of the dipion system. These quantities are essentially those used in the analysis of hadronic dilepton production.

The analysis presented here is motivated by two experimental observations. The first is that a high-p_T π^0 is usually produced as part of a collimated jet of particles [9,10]. The second, to be shown below, is that such a π^0 typically carries 70% or more of the total jet momentum and is very closely aligned with the jet axis [10]. These observations are naturally interpreted in a hard-scattering model where the jet is composed of the fragments of the scattered constituent. The cross-section for high-p_T constituent scattering is determined by the structure functions of the incident protons and the fundamental scattering process, which produce a steeply falling p_T spectrum. When combined with the fragmentation process, this makes it most probable that a single π^0 of transverse momentum p_T arises from a collision in which a parton is produced with transverse momentum p_T' just larger than p_T *). In this picture, the mass of the dipion system is a measure of the centre-of-mass energy of the two partons which undergo the hard-scattering, and the angle of the dipion axis corresponds closely to the direction of the scattered partons. As discussed later, a Monte Carlo calculation gives explicit confirmation of the agreement in this model between the angular distribution of the basic hard-scattering subprocess and the angular distribution of the axis of the final-state dipion system.

The fraction of the total jet momentum taken by the trigger particle, for the "inclusive" and for the "pairs" trigger, has been extracted from the data as follows. The jet direction is approximated by the direction of the trigger particle, in which case $p_T(\text{jet}) = p_T(\text{trig}) + \sum p_x$, where p_x is the component of momentum along the direction of the trigger particle in the plane perpendicular to the incoming protons, and the sum is taken over all charged particles with $p_T >$ > 0.3 GeV/c whose directions lie within

*) This feature of high-p_T particle production was given the somewhat misleading name of "trigger bias" (see Jacob and Landshoff [11]).

a) an azimuthal angle difference of $\pm 60^\circ$ from the trigger particle;

b) $-0.7 < y < 0.7$.

The trigger particle rapidity is restricted to the range $|y| < 0.4$. In terms of the standard variables, $x_e = p_x/p_T(\text{trig})$ and $z = p_T(\text{trig})/p_T(\text{jet})$, $\langle z \rangle = 1/[1 + \langle \sum(x_e) \rangle]$. The large acceptance for charged particles allows us to determine $\langle \sum(x_e)(\text{charged}) \rangle$, which is multiplied by 1.5 to give $\langle \sum(x_e)(\text{all}) \rangle$, assuming that $\langle \sum(x_e)(\text{neutral}) \rangle$ is half $\langle \sum(x_e)(\text{charged}) \rangle$. We note that the approximation of the jet direction by that of the trigger particle is justified for large values of z.

The data on $\langle z \rangle$ for single-particle inclusive triggers is shown in figs. 1 and 2 as a function of $p_T(\text{trig})$ and $x_T(\text{trig})$ $[= 2p_T(\text{trig})/\sqrt{s}]$ for three values of $\sqrt{s}$. Note that as previously stated, the trigger π^0 carries a large fraction of the total jet momentum. It is further seen that $\langle z \rangle$ is not a constant, as a simple scaling model would imply, but depends on both $\sqrt{s}$ and $p_T(\text{trig})$. At a given $p_T(\text{trig})$, $\langle z \rangle$ decreases with increasing $\sqrt{s}$, whilst at fixed $\sqrt{s}$, $\langle z \rangle$ increases with $p_T(\text{trig})$. A scaling form of behaviour is recovered, however, when treating $\langle z \rangle$ as a function of $x_T(\text{trig})$ (fig. 2). Figure 3 shows $\langle z \rangle$ for all events satisfying the "pairs" trigger, with the additional requirement that the two π^0's have an invariant mass above 8 GeV/c^2. For these events, z is calculated for each trigger particle independently. Whilst $\langle z \rangle$ is significantly lower at low $p_T(\text{trig})$ than it is for inclusive triggers, it is still large enough to approximate the jet direction by that of the trigger particle.

Analysis of the "pairs" trigger data will be made using the variables m, P_T of the pair, and $\cos\theta^*$, as previously defined. Figure 4 shows the mean value of P_T for pair masses above 10 GeV/c^2, as found from fits to the observed P_T distribution corrected for apparatus and trigger acceptance [10]. The $\langle P_T \rangle$ may show a tendency to increase slowly with mass and is larger than for lepton pairs [4], as would be expected. For the analysis of the mass and angular distributions, we restrict the P_T range so that $\cos\theta^*$ will more closely approximate the scattering angle of the two particles.

Figure 5 shows the mass dependence of the process $p + p \to \pi^0 + \pi^0 + X$ at the two values of $\sqrt{s}$; the Y interval is from -0.35 to 0.35, and the dipion system is restricted to have $P_T < 1.0$ GeV/c and $|\cos \theta^*| < 0.4$; the data have been corrected for the apparatus acceptance, which is flat over this region and has a value of about 30% *). The quantity plotted is

$$\frac{d\sigma}{dm} = \int_{-0.4}^{+0.4} d \cos \theta^* \int_0^1 dP_T (d^4\sigma/dm\, dY\, dP_T\, d \cos \theta^*) \ . \qquad (1)$$

The data extend from an effective mass of 8 GeV/c^2 up to 16 GeV/c^2 (see also table 1).

In a scaling model, the cross-section can be expressed as the product of three terms: an angular term, a term that depends on $m/\sqrt{s}$ ($\equiv x$), and a term that depends on m.

The first test of scaling is made by simultaneously fitting the mass spectra of fig. 5, obtained at the two values of $\sqrt{s}$, to the form $Am^{-n}G(x)$. The results, using two forms for G(x), are given in table 2. The mass spectra are well consistent with scaling, and the value of n obtained is approximately 6.5 independent of the choice for G(x). The quantity $m^{6.5}\, d\sigma/dm$ is shown in fig. 6, plotted as a function of $m/\sqrt{s}$. When plotted in this way, the data from the two $\sqrt{s}$ are seen to coincide.

The second test of scaling is made by dividing the data into several mass ranges and examining their dependence on $\cos \theta^*$ (figs. 7a and 7b). Fits to the form

$$\frac{d\sigma}{dm\, d \cos \theta^*} = \frac{A'}{m^n} G(x) \left[\frac{1}{(1 - \cos \theta^*)^a} + \frac{1}{(1 + \cos \theta^*)^a} \right] \ldots \qquad (2)$$

in fixed mass bins give the values of a shown in table 3. Note that the P_T range used here is increased at higher masses to improve the statistics; at these

*) An advantage of our choice of kinematic parameters is that it allows the acceptance to be calculated in a model-independent way, event by event.

masses, however, the uncertainty in the definition of cos θ^* is still small and, as will be shown, the increased P_T range has essentially no effect on the value of a obtained. The χ^2 values of the fit are satisfactory and, within the statistical precision, the power a is independent of mass and $\sqrt{s}$. A global fit to the data gives $a = 2.97 \pm 0.05$, with $\chi^2 = 124$ for 116 degrees of freedom. The angular dependence of the data is thus consistent with the scaling and factorization hypothesis. Any systematic variation in calibration across the lead-glass arrays (i.e. with cos θ^*) is estimated to be less than 3% and contributes an additional systematic uncertainty of ±0.2 to the value of a.

We note that our fitting form (2) may be rewritten in terms of Mandelstam variables, treating the dipion effective mass as proportional to the centre-of-mass energy of the original hard-scattering, in the form

$$\frac{d\sigma}{dm\, d\cos\theta^*} = \frac{A''G(x)}{s^b}\left[\frac{1}{t^a} + \frac{1}{u^a}\right], \qquad (3)$$

where $b(= n/2-a) = 0.25 \pm 0.25$ and $a = 3.0 \pm 0.2$.

The form (3) was chosen for its simplicity and symmetry, but cannot be immediately compared to the sum of terms required by constituent models, since many subprocesses are expected to contribute to the reaction studied here. To see how well hard-scattering models of high-p_T production describe our data, we have used a Monte Carlo program based on lowest order QCD. The cross-sections for the basic subprocesses are taken from Combridge et al. [12], and the quark and gluon distributions and fragmentation functions are taken from Buras and Gaemers [13] and Owens et al. [14]. Specifically, the distributions used were

for the sea quark:

$$xS(x,q^2) = \frac{1}{6}(1.21 + 0.613\, s + 0.0764\, s^2)(1-x)^p ,$$

where

$$p = (10 + 1.652\, s + 3.3\, s^2) ;$$

for the gluon:

$$xG(x,q^2) = (2.41 + 3.592\, s + 2.393\, s^2)(1-x)^p ,$$

where

$$p = (5 + 7.201\ s + 3.87\ s^2) \ .$$

For the valence quarks, the u-quark distribution was

$$xU(x,q^2) = 3V(a,b) - V(c,d) \ ,$$

and the d-quark was taken as

$$xD(x,q^2) = V(c,d) \ ,$$

where

$$V(e,f) = (x^e)(1-x)^f\left[\Gamma(e+f+1)/\Gamma(e)\Gamma(f+1)\right]$$

and

$$a = 0.7 - 0.176\ s$$

$$b = 2.6 + 0.8\ s$$

$$c = 0.85 - 0.24\ s$$

$$d = 3.35 - 0.82\ s \ ,$$

and

$$s = \ln\left[\ln\ (q^2/\Lambda^2)/\ln\ (q_0^2/\Lambda^2)\right] \ ,$$

with

$$q_0^2 = 1.8\ (\mathrm{GeV/c})^2 \quad \text{and} \quad \Lambda = 0.3\ \mathrm{GeV/c} \ .$$

The initial-state partons were considered to have Gaussian momentum distributions along two axes transverse to the beam with σ = 700 MeV/c along each axis, and the final-state particles were assigned Gaussian momentum distributions along two axes transverse to the scattered parton direction with σ = 300 MeV/c along each axis. Varying these parameters by 30% has only a small (< 15%) effect on the over-all normalization and produces no change in the shape of the predicted cross-sections. Rather than generating the entire cascade of the scattered constituent into final-state hadrons -- a lengthy and time-consuming process -- the leading final-state particle (from each parton) was selected from a distribution of the form $(1-z)^n$ $\left[z = p_T(\pi^0)/p_T(\mathrm{parton})\right]$ with n = 2 and 3 for the quark and gluon fragmentation f_q and f_g, respectively. To save further computing time, the program only generated π^0's with z above 0.35, since only particles above this value had sufficient p_T

to be accepted in the analysis. The correction to the absolute normalization for particles produced with z below 0.35 was obtained from the figures for leading hadron distribution given by Field and Feynman [15].

Figure 8 shows the relative contributions of the three most important processes: valence-quark valence-quark scattering (qq-qq); gluon valence-quark scattering (gq-gq); and gluon-gluon scattering (gg-gg and gg-qq). Note that the rapid fall in the importance of the gluon terms, as illustrated in figs. 8a and 8b, is not due to the softer gluon fragmentation assumed but to the gluon distribution functions themselves.

Figure 9 shows the cross-section $d\sigma/dm$ [defined in eq. (1)] as measured and as predicted by our Monte Carlo program. Given the simple structure of our model, the level of agreement between our prediction and the data is quite encouraging although the shapes of the two curves are somewhat different. At high mass the agreement is good, whilst at low mass the measured cross-section is significantly higher than predicted. An over-all normalization correction, due for example to an error in the estimate of the fraction of partons which fragment with no particle above $z \equiv 0.35$, will not affect this disagreement. A variety of effects could, however, contribute to the disagreement at lower masses. Apart from the question of the validity of taking the lowest-order terms only*), and the choice of the QCD evolution parameter q^2 **), there is some uncertainty in our knowledge of the gluon distribution and fragmentation functions. As seen in fig. 8, the gluon terms are most important at lower masses; thus a mistake in the assumed gluon distribution would tend to have most effect in this region. In particular, the correctness of the q^2 evolution of this distribution is quite important; as an example, our gluon distribution falls by a factor of almost 2 between a q^2 of 5 $(GeV/c)^2$ and 30 $(GeV/c)^2$ at $x = 0.2$. We should emphasize that our purpose in comparing the data with the Monte Carlo has been simply to demonstrate that a

---

*) The equivalent calculation for the Drell-Yan process needs to be corrected by a factor of between 1.5 and 2.5. See J. Badier et al. [16].

**) The choice $q^2 = t$ was used.

simple QCD approach predicts the observed cross-section within a factor of 2 or so. A variety of forms for the gluon structure functions have been proposed. In particular, harder gluon distributions*), which increase the contribution of the gluon terms, raise the predicted over-all cross-sections by a factor of about 2.

We have compared the angular distribution as measured and as predicted. As mentioned, the agreement between the observed dipion angular distribution and the angular dependence of the hard-scattering subprocess has been checked by Monte Carlo. Figure 10 shows the value of the parameter a obtained from fitting to form (1) the angular distribution of the hard-scattering subprocess as generated by the Monte Carlo program, compared to the values of a obtained from fitting the subsequent dipion distribution. The agreement is typically better than 3%. Figure 11 shows the values predicted by our Monte Carlo program compared with the measured values of a from fits to the observed angular distribution. The typical measured value of a is 3.0 and the agreement is good at all masses. It was our hope to be able to put strong constraints on the relative importance of gluon-gluon scattering, since this has a characteristically flatter angular distribution than the other subprocesses. It turns out, however, that at fixed dipion mass, since q^2 changes with $\cos 0^*$, the gluon distribution itself evolves with $\cos \theta^*$, which has the effect of steepening the actual angular distribution of gluon-gluon scattering from an effective a of 2.4 to a value of 2.7. Thus any alteration of the gluon distribution or fragmentation functions which increases the gluon contribution at dipion masses around 8 GeV/c^2 by as much as a factor of 2, cannot be excluded with the measured angular distributions. We note that the variation of the strong-coupling parameter α_s with q^2, contributes approximately 0.3 units to a. Without this effect, the comparison would be considerably worse.

---

*) As, for example, the gluon distribution given in R. Baier et al. [17].

SUMMARY

We have presented data on the process $p + p \rightarrow \pi^0 + \pi^0 + X$ and compared our measurements with a lowest-order QCD prediction. In this picture the reaction is interpreted as a hard collision between proton constituents. The angular distributions measured can be used to constrain the relative contributions of the various hard-scattering subprocesses within a factor of 2. The cross-section predicted by our Monte Carlo is within a factor of 2 of the observed cross-section for effective masses from 8 to 16 GeV/c^2. The measured angular distributions agree well with the naive QCD predictions at all masses.

Our Monte Carlo calculation shows that the sort of analysis presented here is insensitive to effects such as the "primordial" transverse momenta of the initial-state partons and the transverse momenta involved in the fragmentation process. Considering that here we are comparing an entirely hadronic process with a lowest-order prediction based essentially on data from deep-inelastic lepton scattering, the level of agreement is quite encouraging. We may hope that experiments planned, or in progress at the ISR and Fermilab, will make further tests of this type of analysis, including extension to dependence on particle type and charge where particular subprocesses can be preferentially selected.

We should like to acknowledge the excellent performance of the CERN ISR and the facilities of the CERN Computing Centre which allowed us to accumulate and process the data presented here. We should also like to thank the staff at our respective institutions for their generous support.

REFERENCES

[1] A.L.S. Angelis et al., Phys. Lett. 79B (1978) 505.

[2] A.L.S. Angelis et al., Phys. Scr. 19 (1979) 116.

[3] A.L.S. Angelis et al., Phys. Lett. 87B (1978) 398.

[4] A.L.S. Angelis et al., Phys. Lett. 94B (1980) 106.

[5] A.L.S. Angelis et al., Phys. Lett. 97B (1980) 163.

[6] A.L.S. Angelis et al., Phys. Lett. 98B (1981) 115.

[7] A.L.S. Angelis et al., Phys. Lett. 105B (1981) 233.

[8] R. Baier et al., Z. Phys. C 2 (1979) 265.
J.F. Gunion and B. Petersson, Phys. Rev. D 22 (1980) 629.

[9] F.W. Büsser et al., Nucl. Phys. B106 (1976) 1.

[10] D. Levinthal, Thesis, Columbia University (1980).
J. Yelton, Thesis, University of Oxford (1981).
M. Jacob, Proc. EPS Int. Conf. on High-Energy Physics, Geneva, 1979 (CERN, Geneva, 1980), p. 473, and references therein.

[11] M. Jacob, P.L. Landshoff, Phys. Rep. 48C (1978) 286.

[12] B.L. Combridge et al., Phys. Lett. 70B (1977) 234.

[13] A.J. Buras and K.J.F. Gaemers, Nucl. Phys. B132 (1978) 249.

[14] J.F. Owens et al., Phys. Rev. D 18 (1978) 1501.

[15] R.D. Field and R.P. Feynman, Nucl. Phys. B136 (1978) 1.

[16] J. Badier et al., Phys. Lett. 96B (1980) 422.

[17] R. Baier et al., Z. Physik C., Particles and Fields 6 (1980) 309.

Table 1

Mass cross-section $(\int_{-0.4}^{+0.4} d\cos\theta^* \int_0^1 dP_T\ (d^4\sigma/dm\,dY\,dP_T\,d\cos\theta^*)$

$\sqrt{s}$ = 44.8 GeV	
Mass (GeV/c^2)	Cross-section (cm^2)
8.08	$3.46 \pm 0.28 \times 10^{-34}$
8.33	$3.09 \pm 0.25 \times 10^{-34}$
8.58	$2.1 \pm 0.20 \times 10^{-34}$
8.83	$1.68 \pm 0.20 \times 10^{-34}$
9.08	$1.06 \pm 0.14 \times 10^{-34}$
9.33	$9.37 \pm 1.40 \times 10^{-35}$
9.58	$6.9 \pm 1.00 \times 10^{-35}$
9.83	$3.69 \pm 0.74 \times 10^{-35}$
10.2	$4.03 \pm 0.60 \times 10^{-35}$
10.7	$2.69 \pm 0.49 \times 10^{-35}$
11.35	$1.79 \pm 0.29 \times 10^{-35}$
12.35	$8.63 \pm 1.80 \times 10^{-36}$
13.35	$2.19 \pm 1.00 \times 10^{-36}$
14.35	$1.07 \pm 0.60 \times 10^{-36}$
$\sqrt{s}$ = 62.4 GeV	
8.08	$6.89 \pm 0.15 \times 10^{-34}$
8.33	$5.37 \pm 0.30 \times 10^{-34}$
8.58	$4.59 \pm 0.12 \times 10^{-34}$
8.83	$3.41 \pm 0.10 \times 10^{-34}$
9.08	$2.67 \pm 0.09 \times 10^{-34}$
9.33	$2.11 \pm 0.08 \times 10^{-34}$
9.58	$1.74 \pm 0.07 \times 10^{-34}$
9.83	$1.21 \pm 0.06 \times 10^{-34}$
10.08	$1.16 \pm 0.06 \times 10^{-34}$
10.33	$9.19 \pm 0.54 \times 10^{-35}$
10.58	$6.94 \pm 0.45 \times 10^{-35}$
10.83	$5.51 \pm 0.41 \times 10^{-35}$
11.08	$4.72 \pm 0.38 \times 10^{-35}$
11.33	$3.76 \pm 0.33 \times 10^{-35}$
11.58	$3.46 \pm 0.33 \times 10^{-35}$
11.83	$2.52 \pm 0.27 \times 10^{-35}$
12.2	$2.13 \pm 0.18 \times 10^{-35}$
12.7	$1.62 \pm 0.15 \times 10^{-35}$
13.2	$1.07 \pm 0.13 \times 10^{-35}$
13.7	$8.32 \pm 1.10 \times 10^{-36}$
14.2	$6.24 \pm 1.10 \times 10^{-36}$
14.7	$3.4 \pm 0.66 \times 10^{-36}$
15.2	$2.82 \pm 0.61 \times 10^{-36}$
15.8	$1.14 \pm 0.27 \times 10^{-36}$
16.8	$6.5 \pm 2.10 \times 10^{-37}$
17.8	$7.7 \pm 2.50 \times 10^{-37}$
18.8	$4.7 \pm 2.00 \times 10^{-37}$

Table 2

$G(x) = A\ e^{-bx}$	$G(x) = A\ e^{-bx^2}$
$A = 28.1 \pm 6.0 \times 10^{-28}$ cm^2	$11.6 \pm 2.8 \times 10^{-28}$ cm^2
$n = 6.4 \pm 0.13$	6.55 ± 0.13
$b = 14.2 \pm 0.7$	38.9 ± 1.8
x^2 = 77/73 degrees of freedom	83/73 degrees of freedom

Table 3

$\sqrt{s}$ = 44.8 GeV		$\sqrt{s}$ = 62.4 GeV	
Mass range (GeV/c^2)	a	Mass range (GeV/c^2)	a
8.25- 9.25	3.35 ± 0.2	8- 9	2.8 ± 0.1
9.25-10.25	2.88 ± 0.2	9-10	3.0 ± 0.15
10.25-11.25	2.86 ± 0.3	10-11	3.05 ± 0.15
11.25-12.25	3.29 ± 0.4	11-12	2.85 ± 0.13
		12-13	2.99 ± 0.2
		13-14	3.15 ± 0.2

Figure captions

Fig. 1 : $\langle z \rangle$ versus p_T(trig) for inclusive π^0 production at $\sqrt{s}$ of 31, 44.8, and 62.4 GeV.

Fig. 2 : The same data plotted versus x_T(trig).

Fig. 3 : $\langle z \rangle$ versus p_T for "pairs" events with $m(\pi^0\pi^0) > 8$ GeV/c^2.

Fig. 4 : $\langle P_T \rangle$ versus mass for "pairs" events.

Fig. 5 : $d\sigma/dm$ [as defined in eq. (1)] versus m for events with $P_T < 1.0$ GeV/c.

Fig. 6 : $m^{6.5}\, d\sigma/dm$ as a function of $m/\sqrt{s}$ for $\sqrt{s} = 44.8$ and $\sqrt{s} = 62.4$ GeV.

Fig. 7 : $d\sigma/dm\, d\cos\theta^*$ versus $\cos\theta^*$ for fixed mass bins, a) at $\sqrt{s} = 44.8$ GeV and b) at $\sqrt{s} = 62.4$ GeV.

Fig. 8 : Relative contributions of valence quark-valence quark (qq-qq), gluon valence-quark (gq-gq), and gluon-gluon (gg-gg,gg-qq) scattering. Curves labelled (1) and (2) use gluon fragmentation functions of $(1-z)^2$ and $(1-z)^3$, respectively. a) for $\sqrt{s} = 44.8$ GeV, b) for $\sqrt{s} = 62.4$ GeV.

Fig. 9 : Comparison between measured and predicted cross-sections at $\sqrt{s}$ of 44.8 and 62.4 GeV.

Fig. 10 : A comparison, using Monte Carlo data, of the parameter a (defined in the text) extracted from fits to the angular distribution of the hard-scattering subprocess with a as extracted from the angular distribution of the axis of the dipion system. The comparison is made for events in which P_T is less than 1 GeV/c and also for events in which P_T is less than 2 GeV/c. The plotted points are displaced within each mass bin for clarity only.

Fig. 11 : Values of parameter a from fits to the data and from the Monte Carlo.

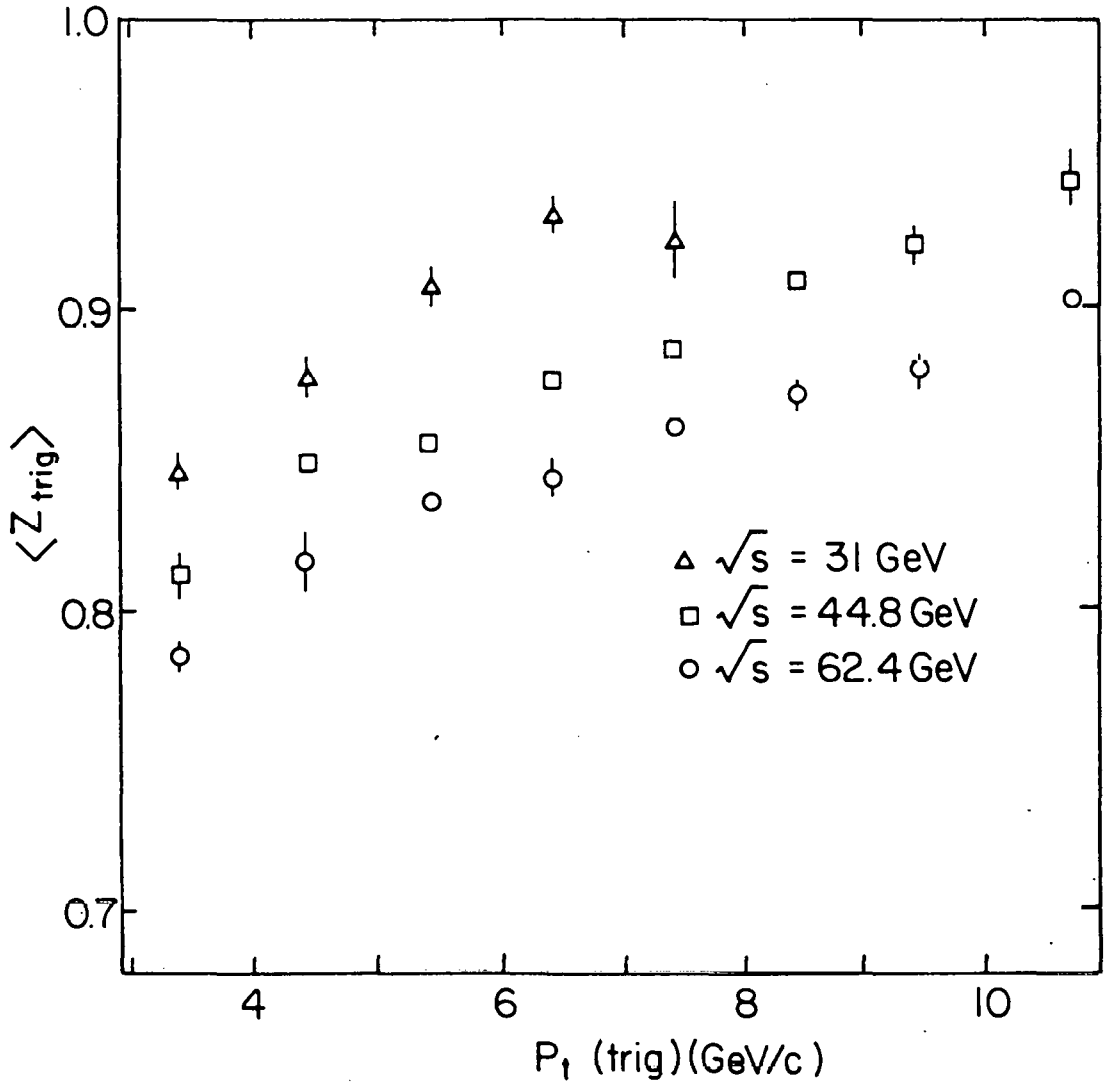
1.0
0.9
0.8
0.7
$\langle Z_{trig} \rangle$
4
6
8
10
P_t (trig)(GeV/c)
$\sqrt{s}$ = 31 GeV
$\sqrt{s}$ = 44.8 GeV
$\sqrt{s}$ = 62.4 GeV

Fig. 1

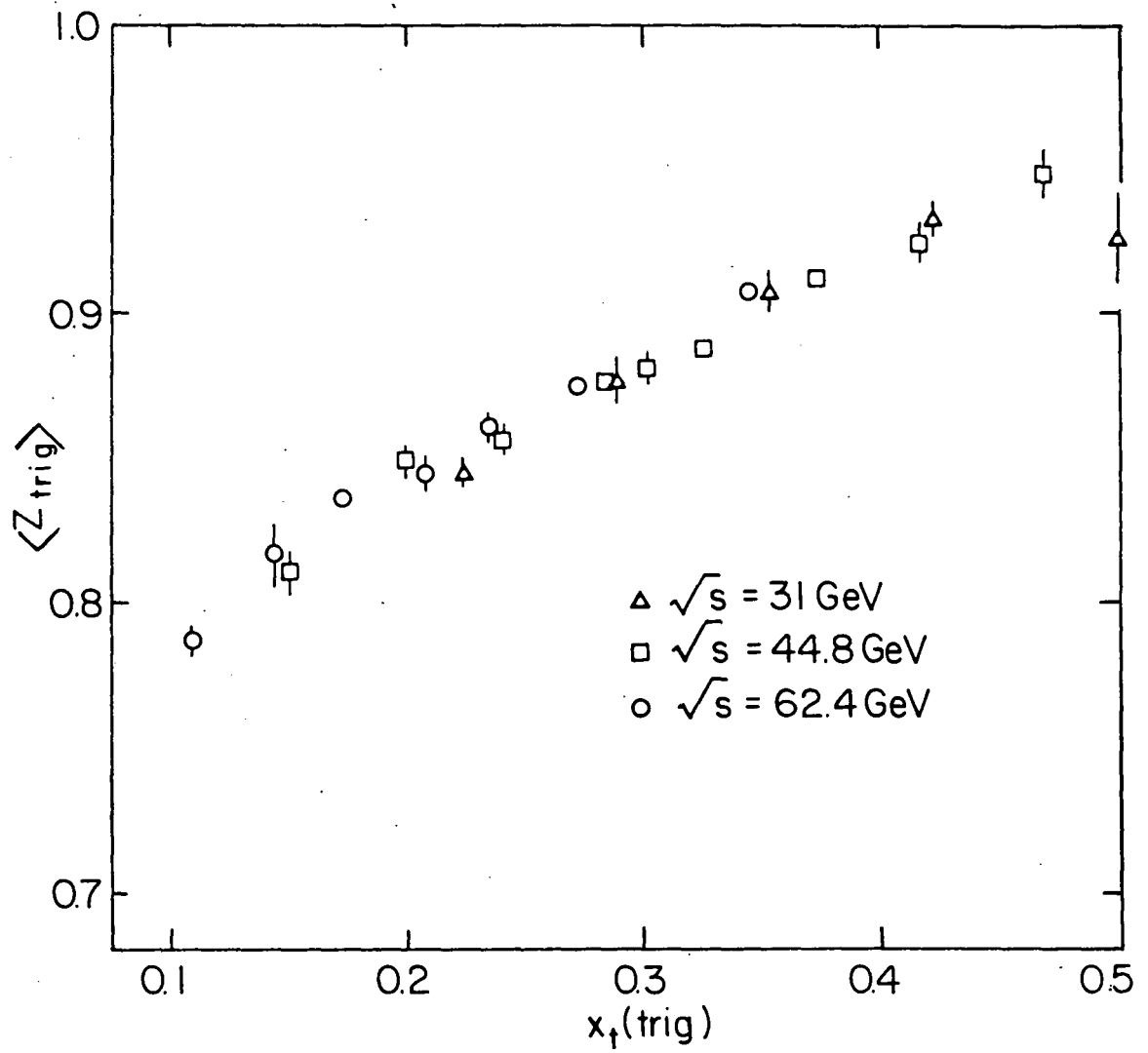
1.0
0.9
0.8
0.7
$\langle Z_{trig} \rangle$
0.1
0.2
0.3
0.4
0.5
x_f(trig)
△ $\sqrt{s}$ = 31 GeV
□ $\sqrt{s}$ = 44.8 GeV
○ $\sqrt{s}$ = 62.4 GeV

Fig. 2

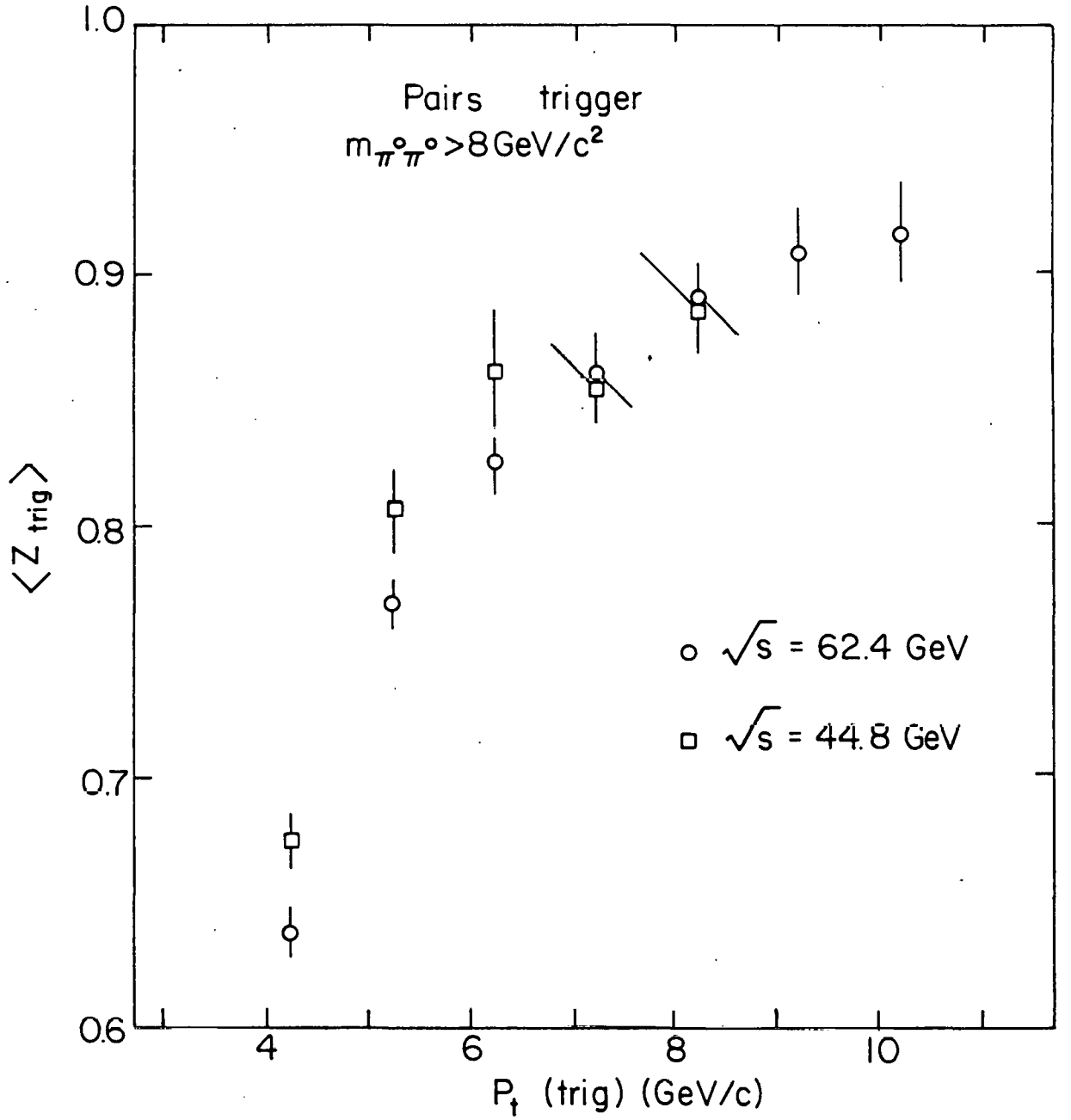
1.0
0.9
0.8
0.7
0.6
Pairs trigger
$m_{\pi^0\pi^0} > 8\,GeV/c^2$
$\langle Z_{trig} \rangle$
$\sqrt{s}$ = 62.4 GeV
$\sqrt{s}$ = 44.8 GeV
4
6
8
10
P_t (trig) (GeV/c)

Fig. 3

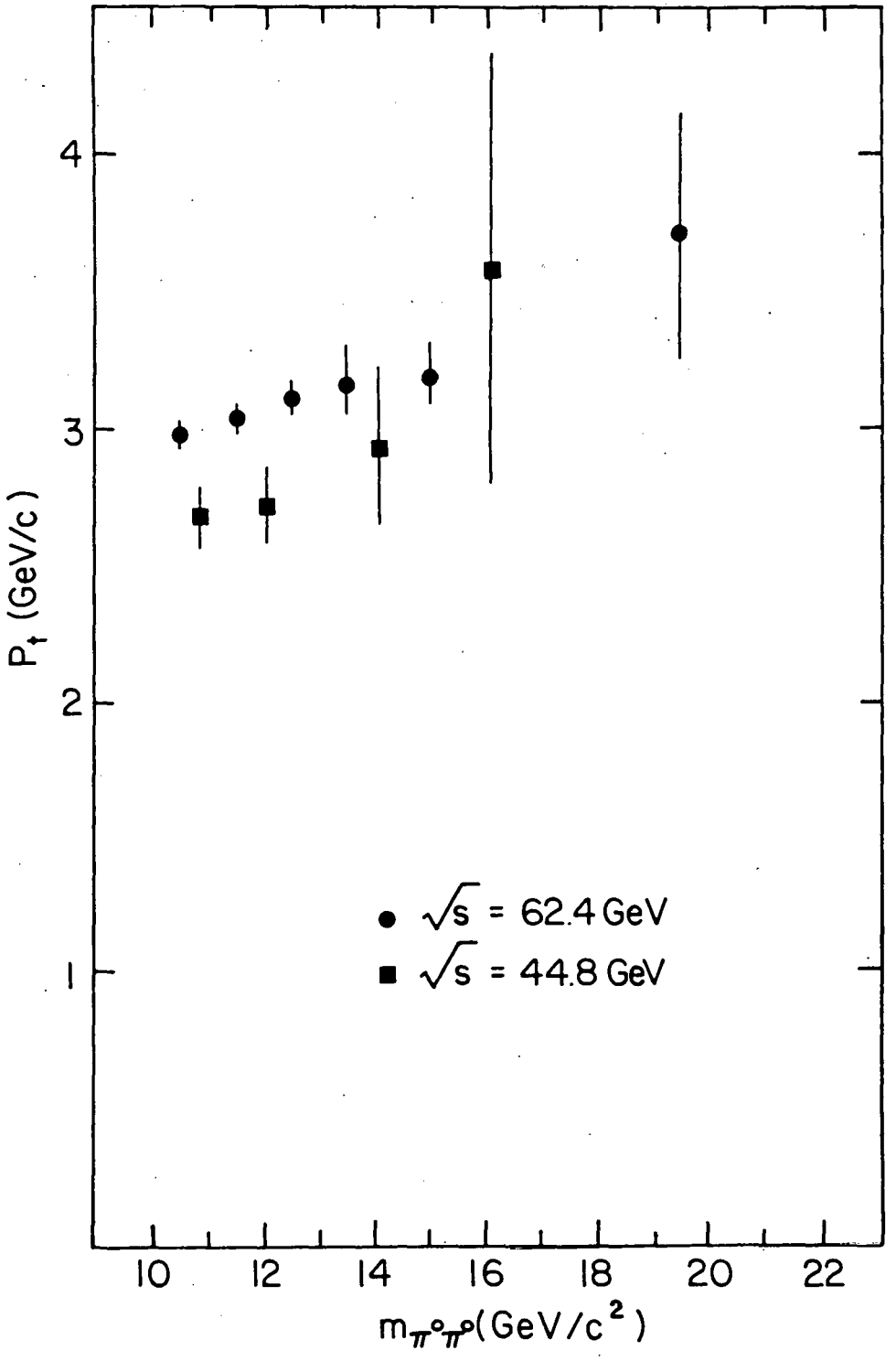
4
3
2
1
P_t (GeV/c)
10
12
14
16
18
20
22
$m_{\pi^0\pi^0}$(GeV/c^2)
● $\sqrt{s}$ = 62.4 GeV
■ $\sqrt{s}$ = 44.8 GeV

Fig. 4

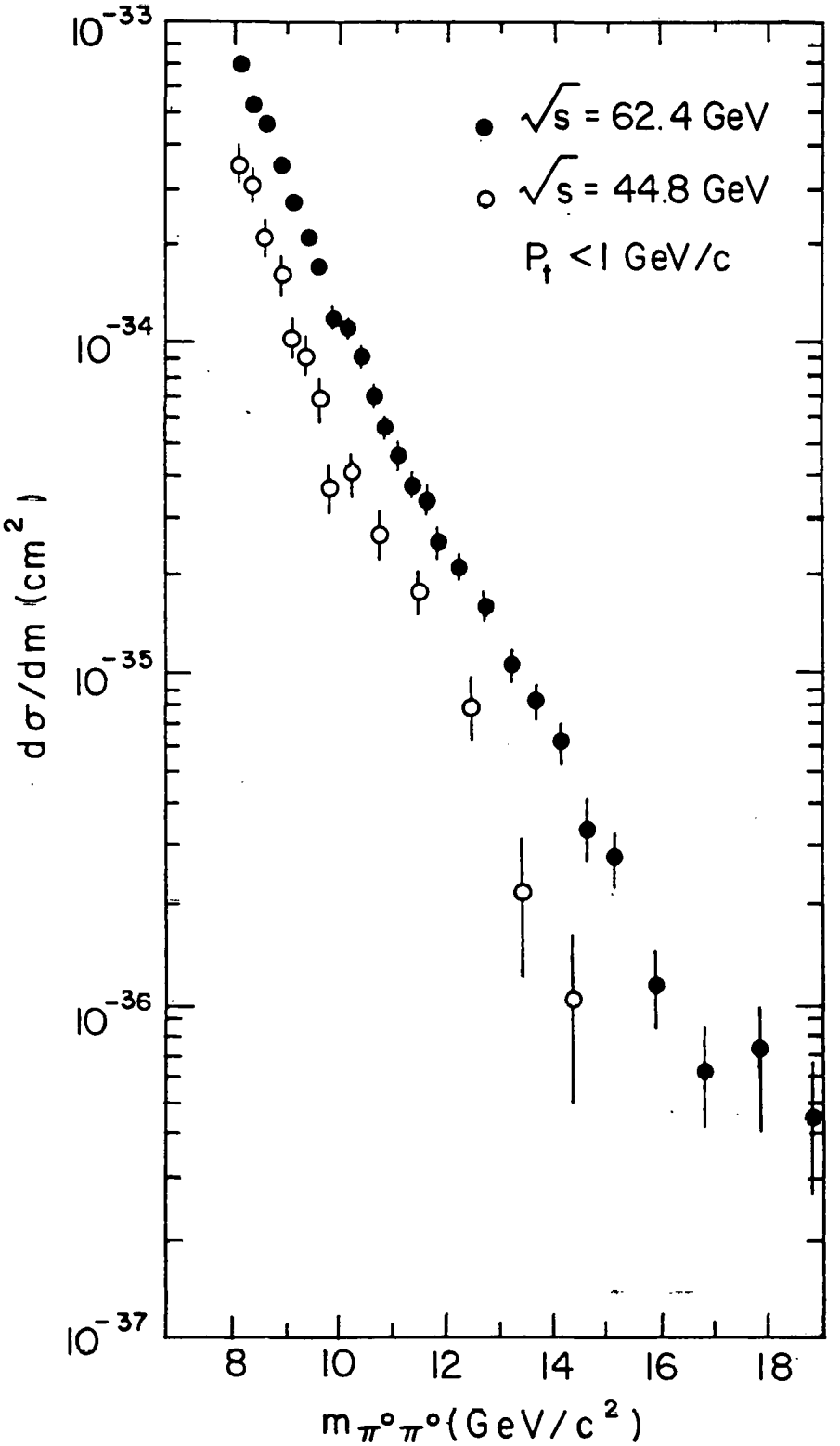
10^{-33}
10^{-34}
10^{-35}
10^{-36}
10^{-37}
$d\sigma/dm\ (cm^2)$
$\sqrt{s}$ = 62.4 GeV
$\sqrt{s}$ = 44.8 GeV
P_t < 1 GeV/c
8
10
12
14
16
18
$m_{\pi^0\pi^0}(GeV/c^2)$

Fig. 5

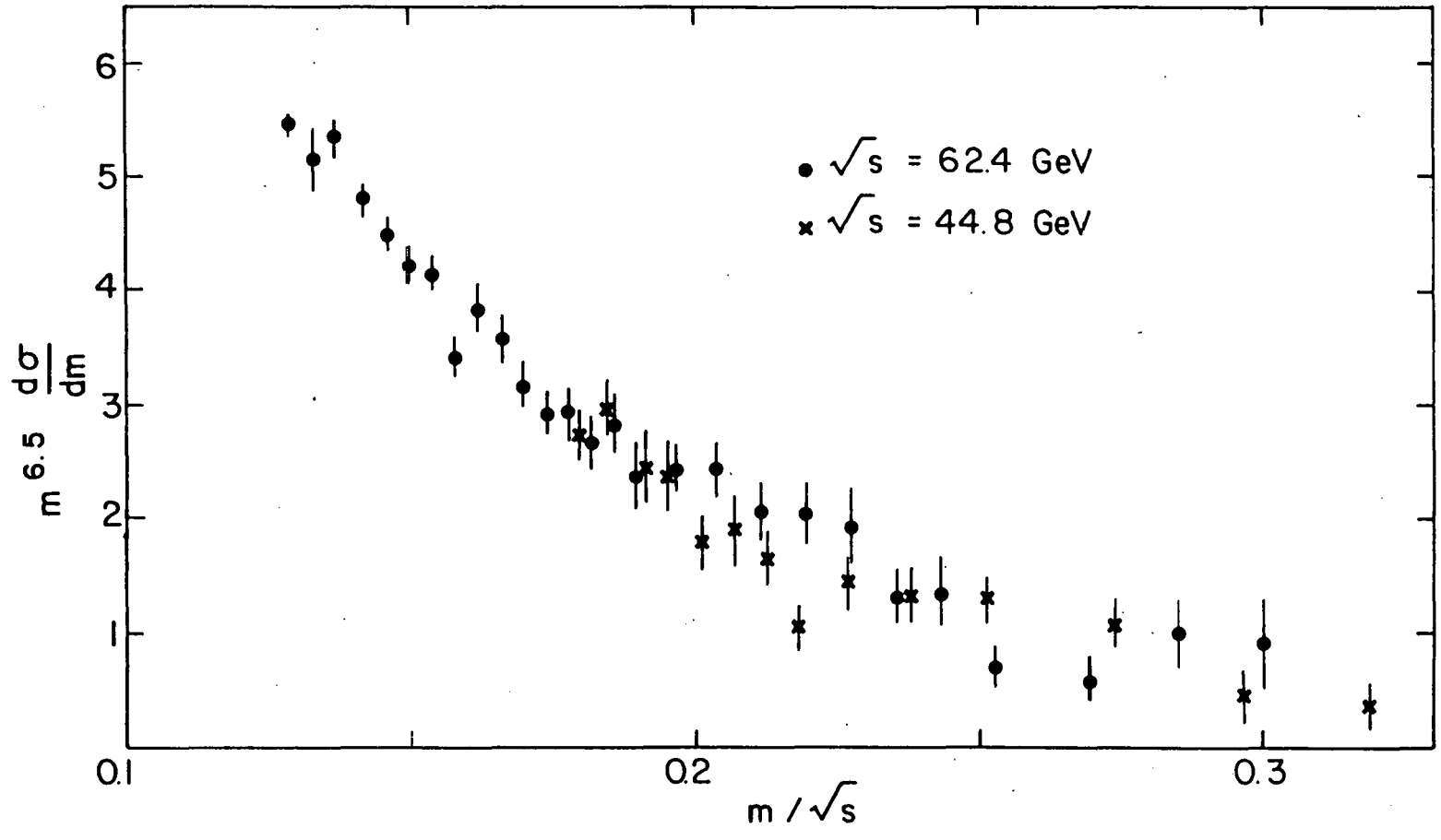

Fig. 6

Di pion angular distributions
$\sqrt{s} = 44.8$ GeV

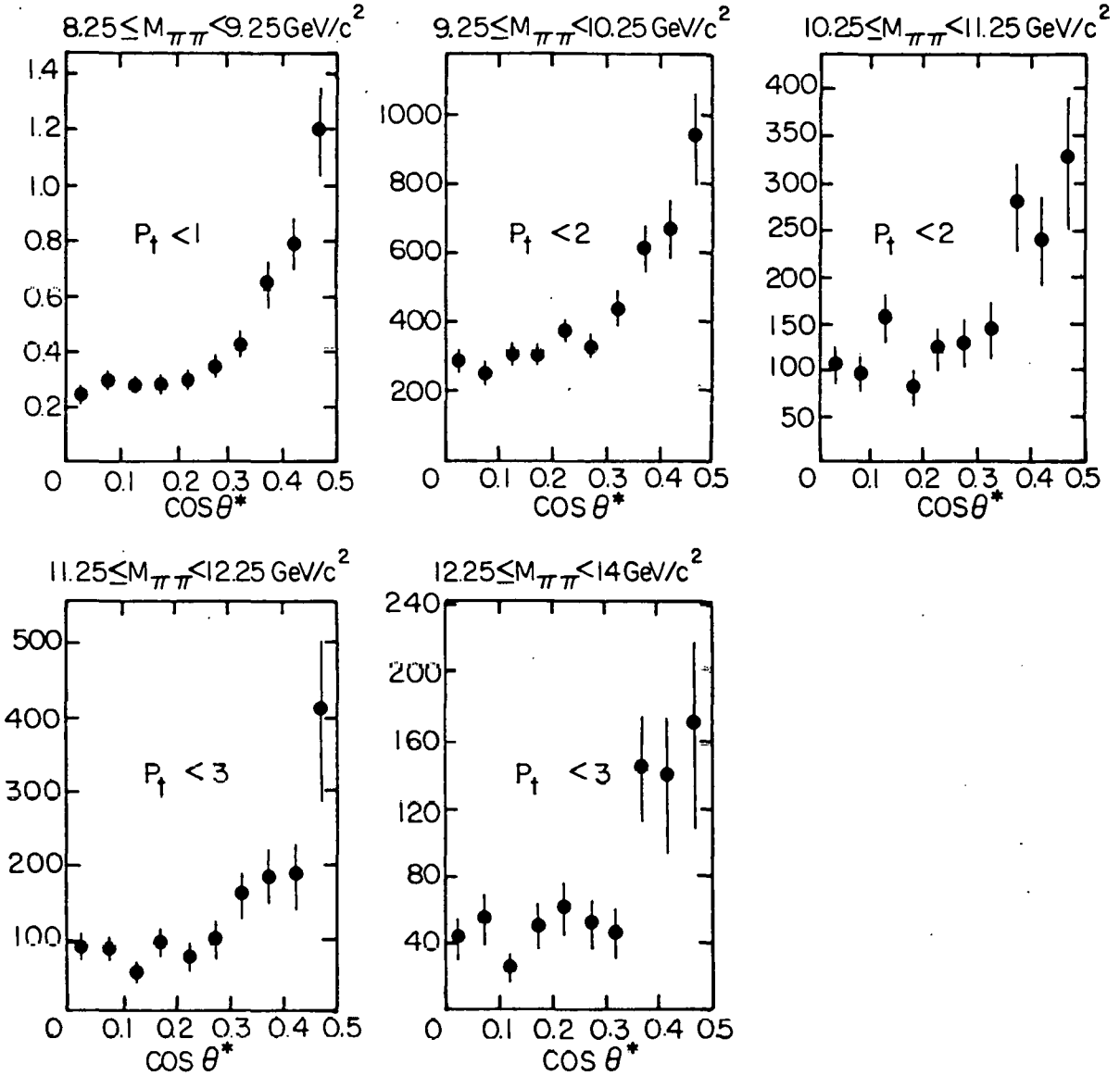

Fig. 7 a)

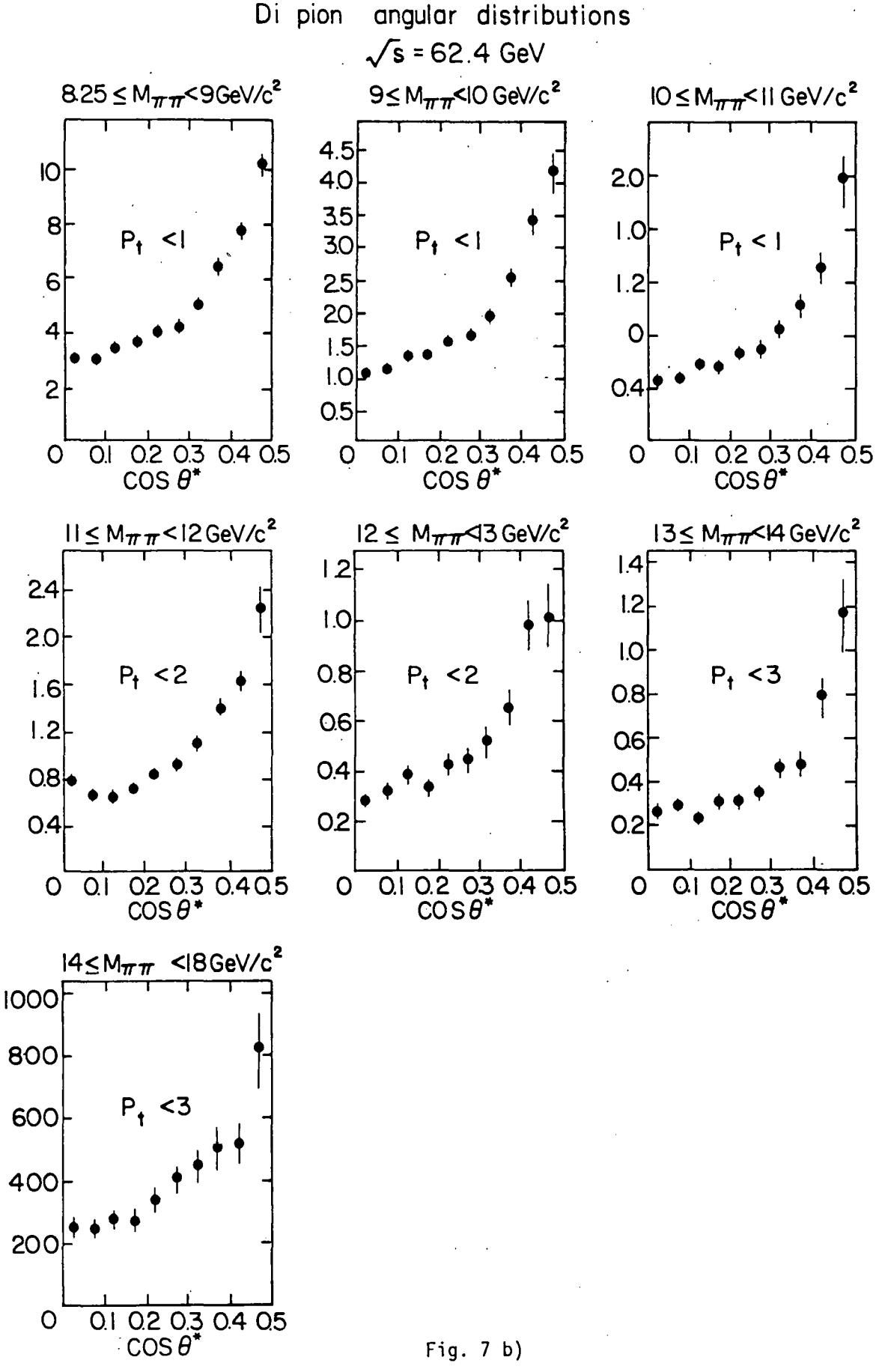
Di pion angular distributions
$\sqrt{s}$ = 62.4 GeV
8.25 ≤ $M_{\pi\pi}$ < 9 GeV/c^2
9 ≤ $M_{\pi\pi}$ < 10 GeV/c^2
10 ≤ $M_{\pi\pi}$ < 11 GeV/c^2
11 ≤ $M_{\pi\pi}$ < 12 GeV/c^2
12 ≤ $M_{\pi\pi}$ < 13 GeV/c^2
13 ≤ $M_{\pi\pi}$ < 14 GeV/c^2
14 ≤ $M_{\pi\pi}$ < 18 GeV/c^2
P_t < 1
P_t < 2
P_t < 3
COS θ*

Fig. 7 b)

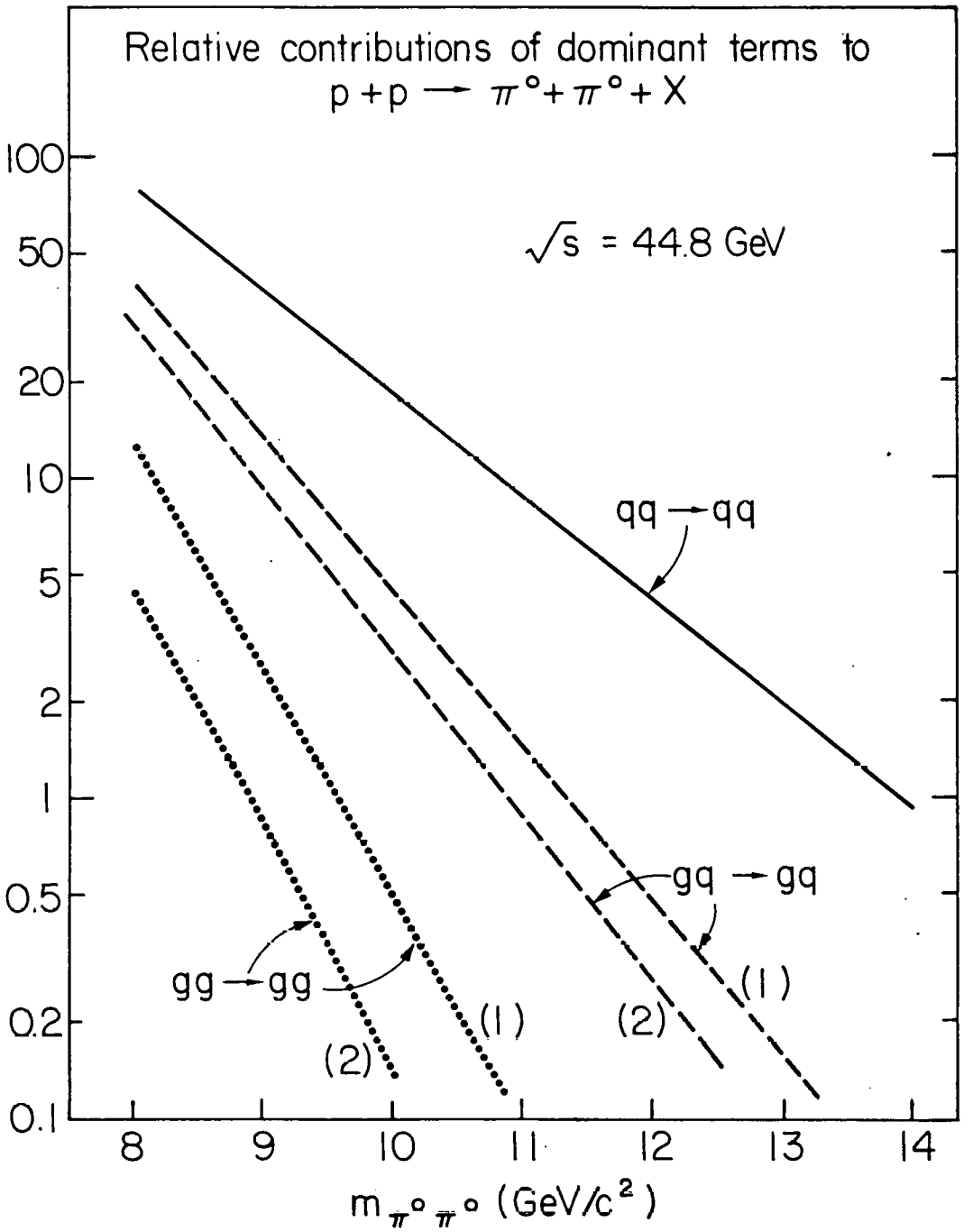
Relative contributions of dominant terms to
p + p → π° + π° + X
√s = 44.8 GeV
qq → qq
gq → gq
gg → gg
(1)
(2)
(1)
(2)
100
50
20
10
5
2
1
0.5
0.2
0.1
8
9
10
11
12
13
14
m π° π° (GeV/c²)

Fig. 8 a)

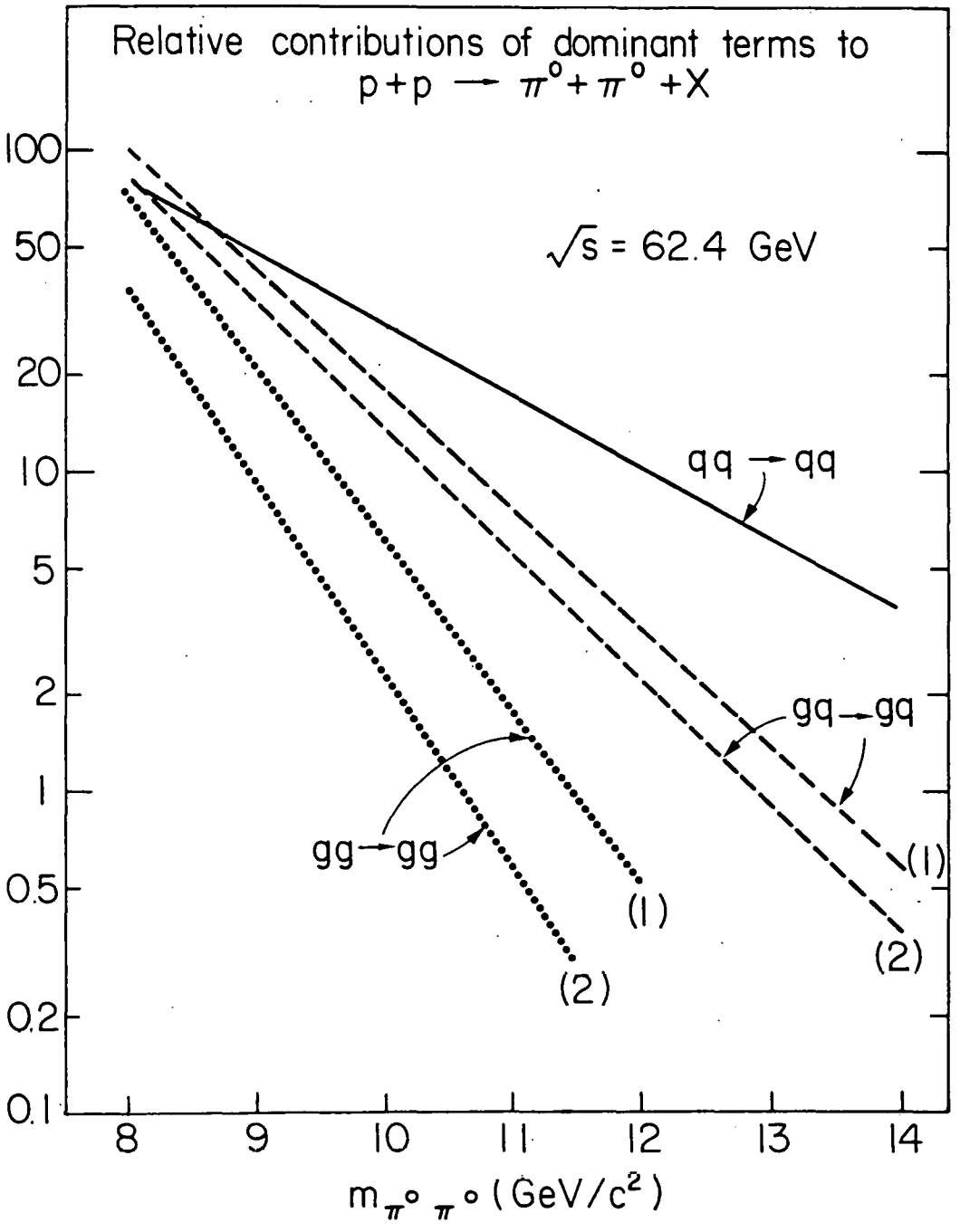
Relative contributions of dominant terms to
p+p → π°+π°+X
√s = 62.4 GeV
qq → qq
gq → gq
gg → gg
(1)
(2)
(1)
(2)
100
50
20
10
5
2
1
0.5
0.2
0.1
8
9
10
11
12
13
14
m π° π° (GeV/c²)

Fig. 8 b)

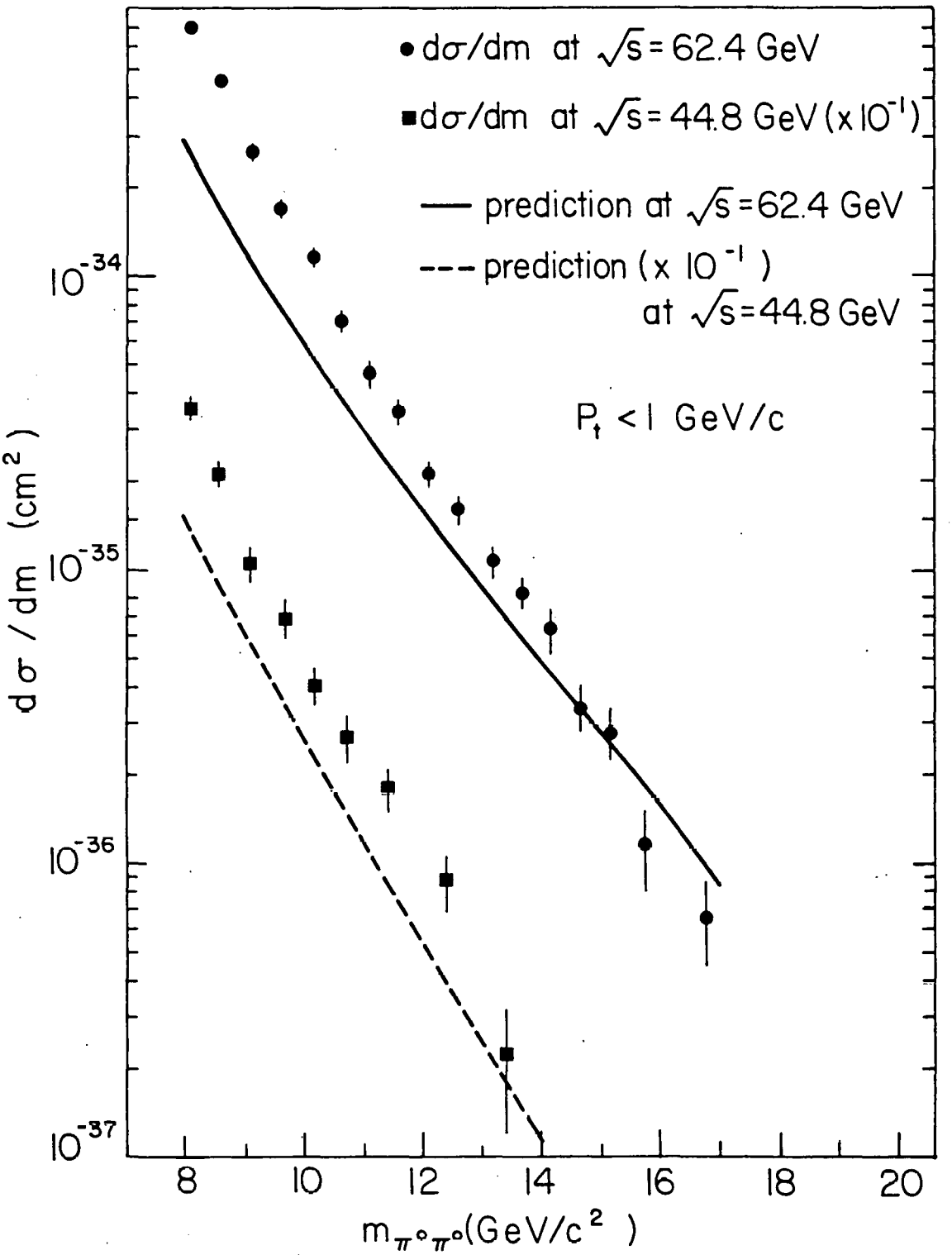
• dσ/dm at √s = 62.4 GeV
■ dσ/dm at √s = 44.8 GeV (x 10⁻¹)
— prediction at √s = 62.4 GeV
--- prediction (x 10⁻¹) at √s = 44.8 GeV
P_t < 1 GeV/c
dσ/dm (cm²)
10⁻³⁴
10⁻³⁵
10⁻³⁶
10⁻³⁷
8
10
12
14
16
18
20
m_π°π°(GeV/c²)

Fig. 9

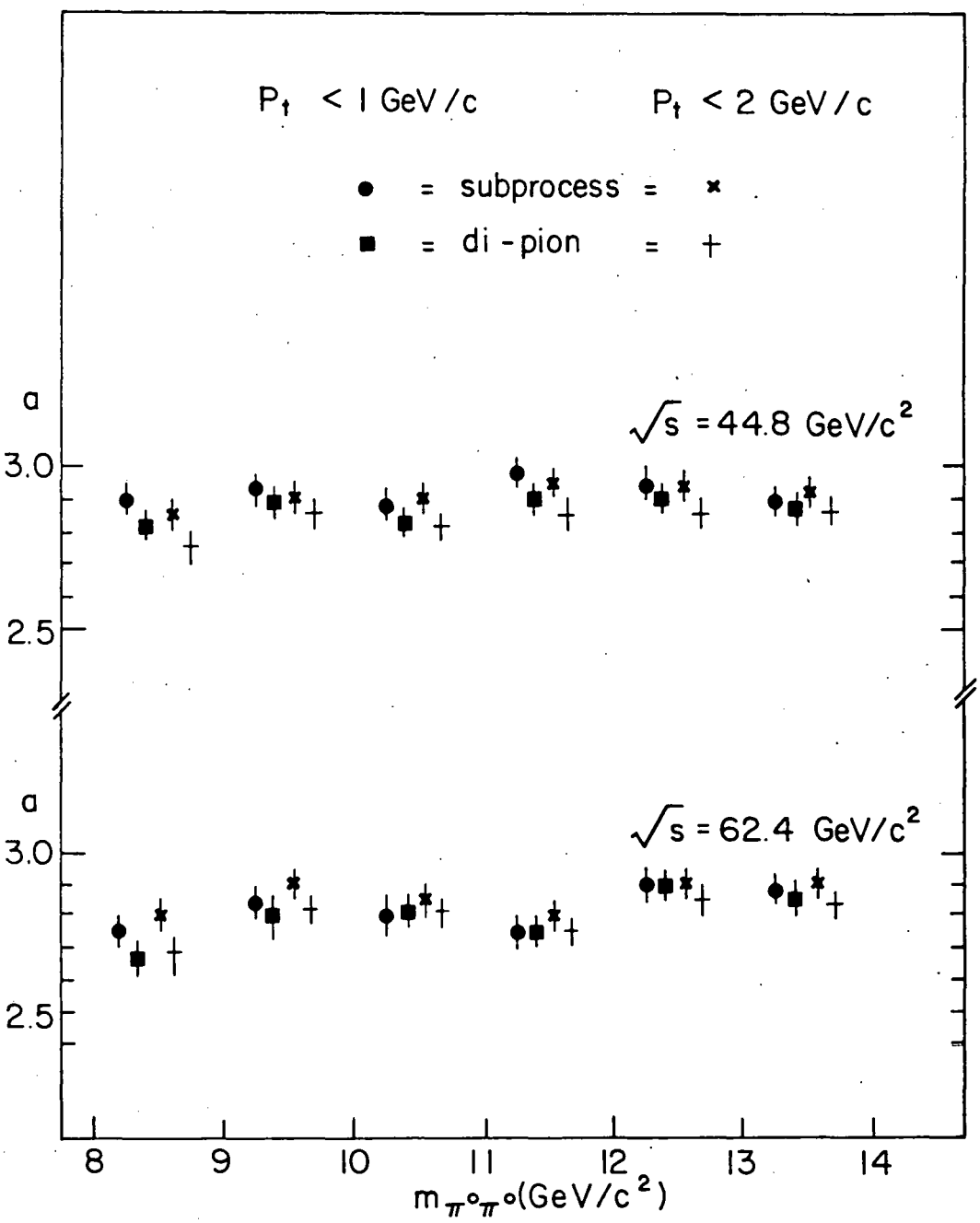
P_t < 1 GeV/c
P_t < 2 GeV/c
● = subprocess = ×
■ = di-pion = +
a
3.0
2.5
$\sqrt{s}$ = 44.8 GeV/c^2
a
3.0
2.5
$\sqrt{s}$ = 62.4 GeV/c^2
8
9
10
11
12
13
14
$m_{\pi^0\pi^0}$(GeV/c^2)

Fig. 10

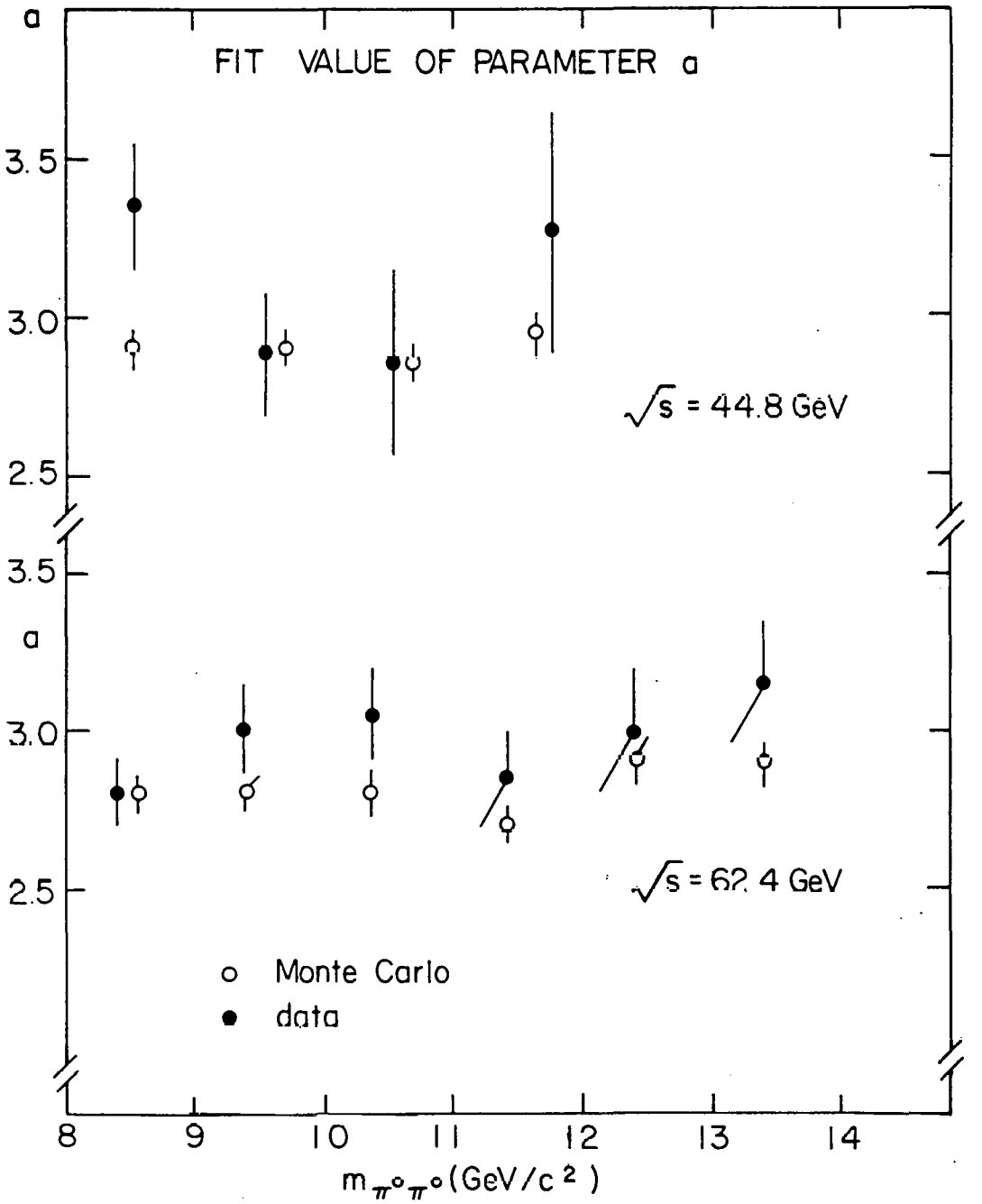
a
FIT VALUE OF PARAMETER a
3.5
3.0
2.5
$\sqrt{s}$ = 44.8 GeV
3.5
a
3.0
2.5
$\sqrt{s}$ = 62.4 GeV
o Monte Carlo
• data
8
9
10
11
12
13
14
$m_{\pi^0\pi^0}$ (GeV/c^2)

Fig. 11